The deep permafrost carbon pool of the Yedoma region in Siberia and Alaska

Jens Strauss,[1] Lutz Schirrmeister,[1] Guido Grosse,[1,2] Sebastian Wetterich,[1] Mathias Ulrich,[3] Ulrike Herzschuh,[1] and Hans-Wolfgang Hubberten[1]

Received 20 September 2013; revised 14 November 2013; accepted 20 November 2013; published 11 December 2013.

[1] Estimates for circumpolar permafrost organic carbon (OC) storage suggest that this pool contains twice the amount of current atmospheric carbon. The Yedoma region sequestered substantial quantities of OC and is unique because its deep OC, which was incorporated into permafrost during ice age conditions. Rapid inclusion of labile organic matter into permafrost halted decomposition and resulted in a deep long-term sink. We show that the deep frozen OC in the Yedoma region consists of two distinct major subreservoirs: Yedoma deposits (late Pleistocene ice- and organic-rich silty sediments) and deposits formed in thaw-lake basins (generalized as thermokarst deposits). We quantified the OC pool based on field data and extrapolation using geospatial data sets to 83 + 61/−57 Gt for Yedoma deposits and to 128 + 99/−96 Gt for thermokarst deposits. The total Yedoma region 211 + 160/−153 Gt is a substantial amount of thaw-vulnerable OC that must be accounted for in global models. **Citation:** Strauss, J., L. Schirrmeister, G. Grosse, S. Wetterich, M. Ulrich, U. Herzschuh, and H.-W. Hubberten (2013), The deep permafrost carbon pool of the Yedoma region in Siberia and Alaska, *Geophys. Res. Lett.*, *40*, 6165–6170, doi:10.1002/2013GL058088.

1. Introduction

[2] Organic carbon (OC) reservoirs of global importance include the ocean, atmosphere, living terrestrial biomass, and terrestrial sediments. Recent studies suggest that 1400 to 1850 Gt of frozen OC are stored in northern high-latitude permafrost soils [*McGuire et al*., 2009; *Tarnocai et al*., 2009]. In the vast northern permafrost Yedoma region that remained unglaciated during the last ice age, alluvial floodplains, hill slopes, and polygonal lowlands [*Strauss et al*., 2012] accumulated OC in Yedoma deposits ≤50 m thick [*Kanevskiy et al*., 2011], while segregated ice (SEI) and massive wedge ice (WI) concurrently formed within the sediments (Figures 1, 2, and S1 in the supporting information (SI)). Yedoma region (Figure 1) permafrost-preserved OC, including ice-rich peat in thaw-lake basins and refrozen lacustrine deposits, is weakly decomposed [*Schirrmeister et al*., 2011] due to fast incorporation into permafrost from the seasonally thawed active layer. Once frozen, organic matter degradation ceases. Observations and models indicate warming and thawing permafrost in many regions [*Romanovsky et al*., 2010], an irreversible process on human timescales [*Schaefer et al*., 2011; *MacDougall et al*., 2012]. Once unlocked by thaw, permafrost organic matter decomposes and CO_2 or CH_4 are produced and released [*Walter et al*., 2006; *Schuur et al*., 2009; *Mackelprang et al*., 2011]. Projections suggest that greenhouse gas emissions from permafrost until 2300 (Representative Concentration Pathways 8.5 scenario) [*Schneider von Deimling et al*., 2012] are comparable in amount to all pre-2000 anthropogenic emissions, thus affecting the global carbon cycle and amplifying surface warming [*McGuire et al*., 2009; *Koven et al*., 2011; *Schaefer et al*., 2011; *Burke et al*., 2012; *Ciais et al*., 2012; *DeConto et al*., 2012; *Schneider von Deimling et al*., 2012; *Schuur et al*., 2013].

[3] Various factors could lead to quick Yedoma region OC mobilization, including active layer thickening [*Schaefer et al*., 2011], widespread thermokarst formation in icy substrates, or accelerated coastal erosion by a sea ice-free Arctic Ocean [*Lantuit et al*., 2012]. However, large uncertainties for the Yedoma region OC pool remain due to scarce data on OC spatial variability, ground ice content, bulk density (BD), and limited knowledge of Yedoma deposit thickness and spatial extent as well as scarce data on presence of other deposits in this region. Because >50% of the modeling-scenario spread in permafrost OC climate response is caused by uncertainties in the permafrost OC pool size [*Burke et al*., 2012], better size estimates of deep frozen OC pools are essential. The objective of this study is to assess the deep OC pool of the Yedoma region (SI, section S1.1.1; potential area of Yedoma-deposit distribution, including thermokarst deposit areas) to reduce quantitative uncertainty concerning thaw-vulnerable permafrost OC.

[4] The Yedoma region OC pool was previously estimated at 450 Gt based on mean 2.56 wt % OC content, mean 25 m deposit thickness, and an estimated 1,000,000 km^2 coverage [*Zimov et al*., 2006]. However, recent studies [*Grosse et al*., 2013] (Figure 1) have shown that Yedoma deposits are fragmented by thermokarst processes and cover only part of the Yedoma region.

Additional supporting information may be found in the online version of this article.

[1]Alfred Wegener Institute Helmholtz Centre for Polar and Marine Research, Periglacial Research Unit, Potsdam, Germany.
[2]Geophysical Institute, University of Alaska Fairbanks, Fairbanks, USA.
[3]Institute for Geography, Leipzig University, Leipzig, Germany.

Corresponding author: J. Strauss, Alfred Wegener Institute Helmholtz Centre for Polar and Marine Research, Periglacial Research Unit, Telegrafenberg A43, DE-14473 Potsdam, Germany. (Jens.Strauss@awi.de)

0094-8276/13/10.1002/2013GL058088

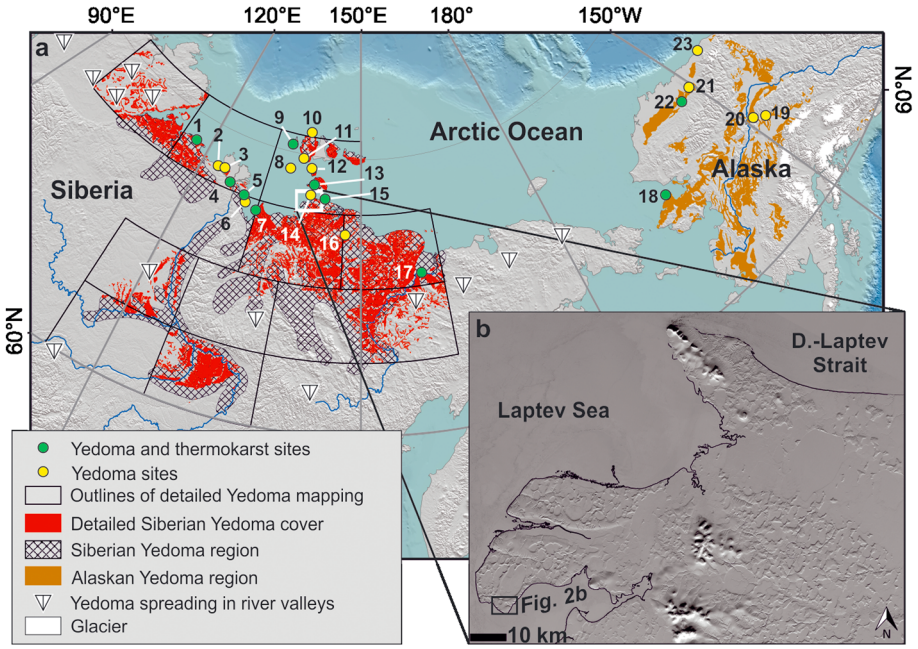

Figure 1. Location of the study sites. (a) Potential [after *Romanovskii*, 1993] and fragmented [*Jorgenson et al.*, 2008; *Grosse et al.*, 2013] area of Yedoma deposits in Arctic and sub-Arctic lowlands, including the studied thermokarst deposit areas. Sites are numbered; 1, Cape Mamontov Klyk; 2, Nagym Island; 3, Khardang Island; 4, Kurungnakh Island; 5, Bykovsky Peninsula; 6, Muostakh Island; 7, Buor Khaya Peninsula; 8, Stolbovoy Island; 9, Bel'kovsky Island; 10 and 11, Kotel'ny Island; 12, Maly Lyakhovsky Island; 13, Bol'shoy Lyakhovsky Island; 14, Cape Svyatov Nos; 15, Oyogos Yar; 16, Kytalyk; 17, Duvanny Yar; 18, Kitluk River; 19, Vault Creek tunnel; 20, Dalton Highway; 21, Itkillik River; 22, Colville River; and 23, Camden Bay. For site 18, only thermokarst deposit samples are available, resulting in 22 Yedoma and 10 thermokarst deposit sites. (b) A panchromatic Landsat-7 image of the wintery Svyatoy Nos and Shirokostan peninsulas (12 March 2012, extent of the white box shown in a), illustrating several granite domes mantled by Yedoma deposits and strong dissection by thermokarst depressions (Landsat data source: USGS EROS Data Center). The black box marks the location of the area shown in Figure 2b.

2. Methods

2.1. Sampling and Organic Carbon Measurement

[5] Twenty-two Yedoma and 10 thermokarst deposit profiles were studied and sampled from river or coastal bluffs exposed by rapid thaw and erosion. In total, 956 individual samples with at least one measured parameter (total organic carbon (TOC), BD, or thickness) were used. The profiles were described and sampled in the frozen state. Samples were extracted manually with hatchet and hammer or hand drills. Samples were kept cooled or frozen and were transported to laboratories for further analysis. TOC samples were measured with a carbon-nitrogen-sulphur analyzer (Elementar Vario EL III) or a TOC analyzer (Elementar Vario Max C).

2.2. Bulk Density Calculation

[6] For BD and SEI calculation, samples were weighed in wet and ovendry state during field expeditions. BD (10^3 kg/m^3) was then calculated using its inverse relationship with porosity (ϕ, equation (1))

$$\mathrm{BD} = (\phi - 1) \times (-\rho_s) \quad (1)$$

whereas ρ_s is the solid fraction density. Because pore volume is assumed to be ice saturated, the pore volume can be directly inferred from SEI. In addition, 133 direct BD measurements were conducted in the field lab by determining the volume of frozen samples extracted from exposures with the Archimedes Principle, i.e., quantifying the water volume displaced by the frozen sample in a glass beaker filled with water. After freeze-drying in the laboratory (Sublimator 3-4-5, ZIRBUS Technology), the SEI and BD were calculated.

2.3. Wedge-Ice Volume Calculation

[7] Wedge-Ice Volume (WIV) was calculated using equations (S4) and (S5) (SI, section S1.4.1). For epigenetic ice wedges, it is assumed that a frontal cut of an ice wedge has a shape of an isosceles triangle (Figure S1, right side). For syngenetic Yedoma deposit ice wedges, we deduced an equation (S5), assuming that a frontal cut of this ice wedge type is rectangular in shape (Figure S1, left side). WI width is based on field measurements extracted from the literature. The Yedoma and thermokarst deposit ice-wedge polygon sizes were determined by mapping very high resolution satellite imagery for four study sites, (SI, section S1.4.2).

2.4. Statistical Methods

[8] Calculations of carbon budget and OC density are based on bootstrapping techniques, i.e., using resampled (10,000 times) observed values (TOC, BD, WIV, thickness) and deriving the mean afterward. Because TOC and BD are genuinely correlated, we used paired values in the resampling process. For that purpose, the missing BD values were calculated using an exponential function ($\mathrm{BD} = 1.126^{-0.0601 \times \mathrm{TOC}}$) that was fitted to those data for which both values were available. After bootstrapping the population of observation (called "observation-based"), the mean was derived. In addition, we

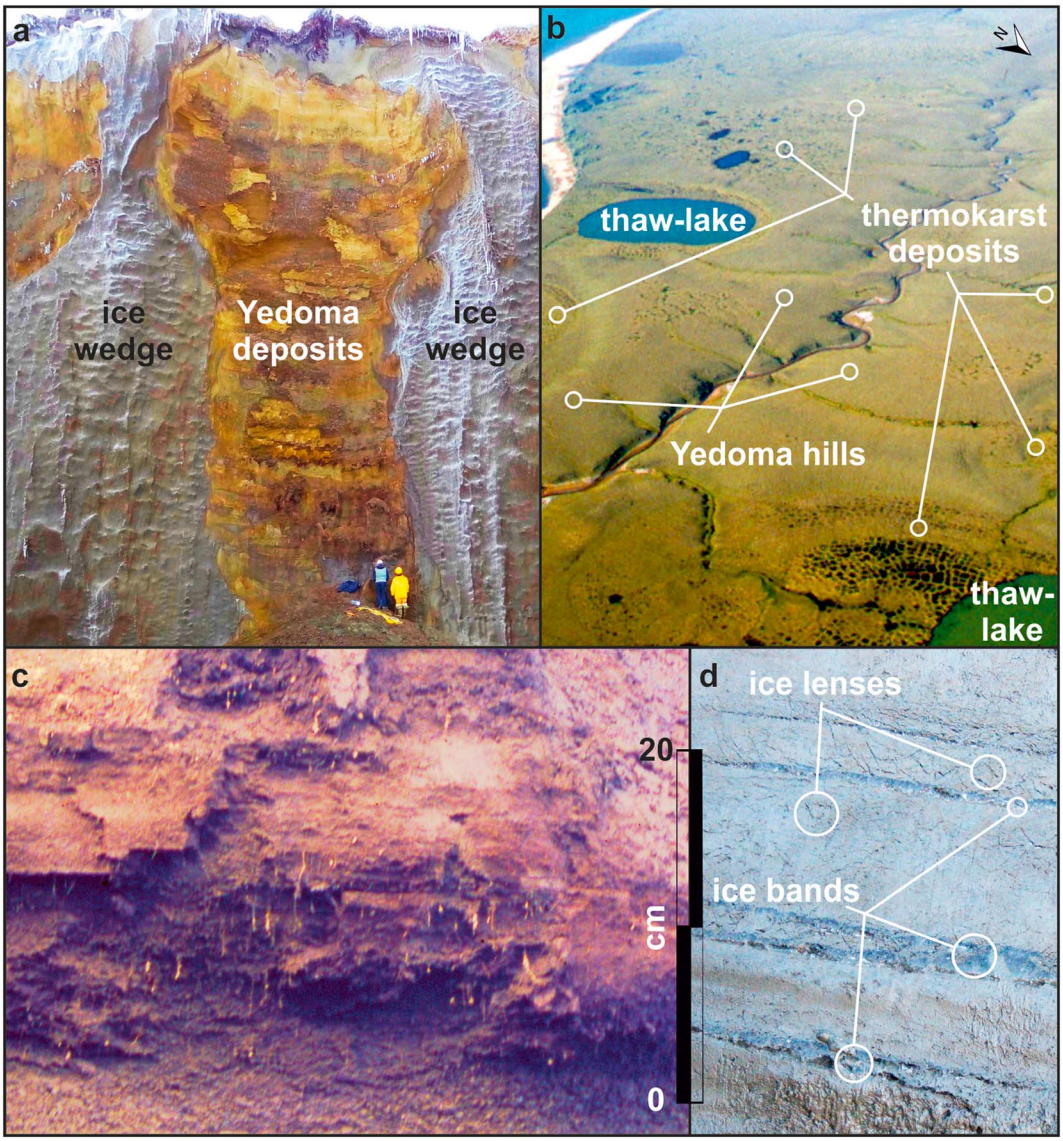

Figure 2. Pictures of studied deposits. (a) Yedoma deposits with wedge ice (WI) exposed at the Itkillik River, Alaska (Figure 1, site 21, photo from *J. Strauss* [2012]); (b) photo of a Yedoma-thermokarst landscape on Shirokostan Peninsula, Laptev Sea (black box in Figure 1b, photo from *L. Schirrmeister* [1999]); (c) example of fossil root-bearing Yedoma deposits from Bykovsky Peninsula, Laptev Sea (Figure 1, site 5, photo from *L. Schirrmeister* [1998]); and (d) example of segregated ice (SEI) (ice lenses and ice bands) at Buor Khaya Peninsula (Figure 1, site 7, photo from *J. Strauss* [2010]).

tested an alternate approach using bootstrapping of single variable means before budget calculation (presented in SI section S1.7) to ease the comparison of results to those derived by previous upscaling studies. Because using single value estimates reduces the variability (SI section S1.7) of the obtained distribution, we choose this observation-based method to have a conservative uncertainty range of OC carbon budget from the Yedoma region. The error estimates in this study represent the 16th and 84th percentiles to reflect the standard deviation which is typically presented in comparable studies (with the assumption of normal distribution). Computations were performed using R software (boot package).

3. Results

[9] The Yedoma region permafrost OC pool largely consists of OC in remaining Yedoma deposits (Figure 2a) and refrozen thermokarst deposits (Figure 2b), including mineral sediments, peat, WI, and SEI (Figures 2a, 2c, and 2d). Other nonperennially frozen OC pools, such as active layer or lake and river sediments, are not included in our study.

3.1. Data and Statistical Methods

[10] Using a data set of 956 frozen samples from 23 Siberian and Alaskan study sites (Figure 1), we measured and modeled the primary parameters (Figure 3) necessary to quantify the overall frozen OC pool, including thickness, spatial coverage, BD (including SEI volume (SEIV)), WI volume (WIV), and total OC (TOC) content of Yedoma and thermokarst deposits of the Yedoma region (SI Tables S1–S5). For calculation, we used equation (2) as follows:

$$\text{OC budget (Gt)} = \frac{\text{thickness (m)} \times \text{coverage (m}^2\text{)} \times \text{BD (10}^3\text{kg/m}^3\text{)} \times \frac{100-\text{WIV}}{100} \times \frac{\text{TOC}}{100}}{1,000,000,000} \quad (2)$$

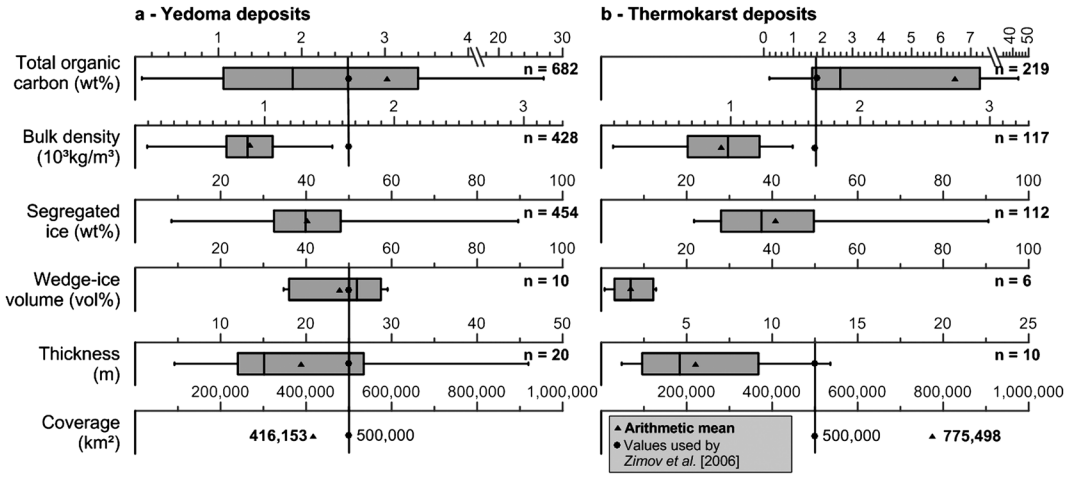

Figure 3. Box plots of the key parameters for (a) Yedoma and (b) thermokarst deposit organic carbon estimation. The literature estimate [*Zimov et al*., 2006] is given by the vertical black line for comparison. Note the different axis scale in Figures 3a and 3b for total organic carbon (TOC) and thickness. Tables S2–S5 (SI) contain these parameters with uncertainty estimates.

[11] Because of high inherent (spatial) heterogeneity and nonnormal input parameter distributions (Figure 3 and S5), we used and report observation-based bootstrapping mean values (rather than simple means) for OC budget calculation and error estimation. For comparison with previous studies, we use our parameter data set and also calculate a pool based on the simple arithmetic mean (SI section S1.8 and Table S1).

3.2. Biogeochemical and Physical Parameters

[12] Mean TOC for Yedoma deposits in Siberia and Alaska is $3.0+1.6/-2.2$ wt % and $6.5+3.9/-5.0$ wt % of the thermokarst deposits, respectively. The BD calculation includes SEI [*Strauss et al*., 2012] (SI, 1.3). Direct measurements on 92 Yedoma and 41 thermokarst deposit samples and calculated values for an additional 334 Yedoma and 76 thermokarst deposit samples (SI, Figure S2) yielded a BD mean of $0.88+0.26/-0.25$ 10^3 kg/m^3 and $0.93+0.33-/0.38$ 10^3 kg/m^3 for Yedoma and thermokarst deposits, respectively, comparable to earlier estimates of 0.98 10^3 kg/m^3 for Yedoma deposits [*Dutta et al*., 2006].

[13] To accurately estimate WIV, a three-dimensional assessment of ice-wedge polygons and WI structures would be necessary. Neither geophysical nor any other technique is available to directly derive such data for deep syngenetic WI. Indirect approaches include WIV estimation from coastal or riverine bluffs [*Kanevskiy et al*., 2011], or remote-sensing and field survey estimations of polygon sizes combined with WI width data. Using this latter approach (SI, section S1.4, Figures S3–S4, and Table S6), we assume a mean $4.0+0.5/-1.4$ m Yedoma deposit WI width and $1.7+1.1/-0.9$ m thermokarst deposit WI width and a mean $13.0+0.4/-1.4$ m Yedoma deposit polygon diameter and $22.1+1.1/-1.8$ m thermokarst deposit polygon diameter (SI, Table S6). Accordingly, the mean Yedoma deposit WIV is 48 vol %, while younger Holocene thermokarst deposits contain 7 vol % WIV due to smaller ice wedges. The sum of SEIV plus WIV equals a mean total volumetric ground ice content of ~82 vol % for Yedoma and ~67 vol % for frozen thermokarst deposits. When this ground ice thaws in a warmer climate, substantial surface subsidence will ensue.

[14] To best approximate deposit thickness, we used the mean profile depths of the sampled Yedoma and thermokarst deposits. The Yedoma base was reached at 12 out of 20 of our study sites. Hence, Yedoma thickness is potentially underestimated. The mean 19.4 m Yedoma deposit thickness is about 4 times larger than the mean 5.5 m thermokarst deposit thickness. Due to lack of sufficient samples and spatial variability, we do not include any OC pools below Yedoma and below frozen thermokarst deposits in our calculation, which potentially contain relevant amounts of carbon [*Schirrmeister et al*., 2011].

3.3. Yedoma Region Coverage

[15] Using a digital Siberian Yedoma region map [*Romanovskii*, 1993] and the distribution of Alaskan ice-rich silt deposits equivalent to Yedoma [*Jorgenson et al*., 2008], we calculated the core Yedoma region extent as ~1,387,000 km^2 (Figure 1a, SI section S1.5). Yedoma deposit distribution is discontinuous due to thermo-erosion and thermokarst processes (Figure 1b). Data from local- and regional-scale analyses of Yedoma deposit versus thermokarst-affected areas (SI, 1.5 and Tab. S7) indicate that ~70% of the Yedoma region area is affected by degradation. The remaining Yedoma deposit extent is ~416,000 km^2. We further estimate that ~10% of the Yedoma region is covered with lakes and rivers and thus underlain by unfrozen deposits (150,000 km^2) and ~4% is covered with other deposits including deltaic and fluvial sediments (50,000 km^2), leaving ~56% (775,000 km^2) of the Yedoma region covered by frozen thermokarst deposits (Figure 2b and SI, section S1.5) in drained thermokarst lakes.

3.4. Inventory Estimations

[16] Combining all available spatial, physical, and biogeochemical parameters (equation (2), Figure 3), we calculated the Yedoma deposit frozen OC pool as $10+7/-6$ kg/m^3 and thermokarst deposits as $31+23/-18$ kg/m^3. WIV is included in this calculation. To show OC density separate from wedge ice for comparability with previous studies, the Yedoma deposit frozen OC pool contain $19+13/-11$ kg/m^3 and thermokarst deposits $33+25/-19$ kg/m^3 when excluding the WIV. Adding the total stored Yedoma deposit OC, $83+61/-57$ Gt, and the

frozen thermokarst deposit OC, 128 + 99/−96 Gt, the total frozen Yedoma region contains 211 + 160/−153 Gt OC (not including active layer nor deeper organic matter deposits below Yedoma or frozen thermokarst deposits). Inferred 16th and 84th percentiles (Yedoma: 22 Gt, 140 Gt; thermokarst: 29 Gt, 224 Gt) are markedly large because of our conservative (observation-based) approach using all measurements for bootstrapping and deriving the mean afterward. The use of single-value estimates such as mean (SI 1.7) reduces the variability of the obtained distribution.

4. Discussion

[17] Our results suggest that we must reconsider whether Yedoma or thermokarst deposits constitute the dominant current Yedoma region OC pool. Moreover, it is essential to make appropriate statistical assumptions previous to the inventory calculations, because a calculation based on observation-based bootstrapping mean values results in a ~40% smaller inventory compared to simple mean approach (Table S1).

[18] The previous estimate [*Zimov et al*., 2006] suggests that 60% of the Yedoma region OC is stored in Yedoma deposits and 40% in thermokarst deposits. Our study reveals the reverse ratio, 40% is stored in Yedoma deposits and 60% in frozen thermokarst deposits. The total Yedoma region frozen OC represents a substantial pool of ancient thaw-vulnerable ice-rich OC deposits. For comparison, global plant biomass contains 350–540 Gt OC [*McGuire et al*., 2009]. Thaw-related Yedoma region OC release will potentially affect large-scale carbon cycling. Paleoclimate models [*Ciais et al*., 2012; *DeConto et al*., 2012] reveal the influence of permafrost OC thaw on Earth's past climate. *Ciais et al*. [2012] found that 10,000,000 km^2 of thawing Eurasian tundra could at least partly constitute the missing cause of an ice-core-inferred 100 ppm atmospheric CO_2 increase during the Pleistocene-Holocene transition. Our calculated 211 Gt Yedoma region OC pool is entirely vulnerable to thaw. When OC will be released, it is presently unclear due to complex positive and negative climate feedback. Nevertheless, if even 20% of this frozen OC pool is emitted as CO_2, in the long term, ~10 ± 7 ppm atmospheric CO_2 increase could result (SI, 1.6, calculation according to *Battle et al*. [2000] and *Schneider von Deimling et al*. [2012]). In this calculation OC emission as CH_4 could not be included because of various uncertainties and unknowns, e.g., a landscape-level carbon dioxide to methane emission ratio.

[19] For further evaluation of OC pool relevance, two questions are important regarding subsequent soil OC mobilization: How was OC incorporated originally (OC source/quality) and what are the OC release trajectories and timescales (OC vulnerability)? Before OC refreezes, it accumulates in the active layer and transition zone above permafrost, either directly by cryoturbation and root growth or indirectly via sediment burying. Cold soils near the permafrost table thaw for only a short time in summer, and organic matter decomposition is severely limited, contributing to the generally high OC content of permafrost-affected soils [*Tarnocai et al*., 2009; *Grosse et al*., 2011]. Evidence of rapid OC preservation in Yedoma deposits includes in situ ancient grass roots (Figure 2c) and well-preserved mammal carcasses. Frozen thermokarst deposits are generally more heterogeneous than Yedoma deposits, as revealed by considerable scattering in TOC data (Figures 3 and S5). Some thermokarst deposits formed in lakes that drained; sediments subsequently refroze and terrestrial peat accumulated over time. Hence, reworked late Pleistocene and Holocene OC and in situ growing organic matter are important contributors to thermokarst deposit OC, resulting in a mean TOC content (6.5 wt %) twice as high compared to Yedoma deposits (3.0 wt %). Since not all Yedoma region organic matter is equally vulnerable to post-thaw decomposition, microbial turnover rates must be known to quantify future OC fluxes. Labile organic matter easily undergoes microbial turnover, but more complex compounds are more inert [*Dutta et al*., 2006; *Burke et al*., 2012; *Lee et al*., 2012]. Organic matter decomposition vulnerability measured by mineralization rates is slightly higher for Yedoma deposits than for thermokarst deposits [*Knoblauch et al*., 2013], because portions of refrozen thermokarst organic matter decomposed under originally unfrozen conditions. Frozen thermokarst deposits 2–3°C warmer than adjacent Yedoma deposits [*Romanovsky et al*., 2010] have been found, suggesting that frozen thermokarst deposits may thaw before Yedoma deposits and the thermokarst OC pool may be affected earlier by Arctic warming. Thaw processes will cause WI melting, subsidence, and rapid erosion. Based on total volumetric SEI and WI content, surface subsidence of ~50–70% is possible, exposing deep OC pools on short timescales. Exposure to sunlight and thaw stimulates bacterial decomposition [*Cory et al*., 2013]. In addition, the development of new and expansion of existing thermokarst lakes in ice-rich deposits may lead to increased release of CH_4 formed in lake sediments and expanding thaw bulbs under lakes [*Walter et al*., 2006].

[20] Most climate model projections either ignore or underestimate the potential atmospheric impact of permafrost OC release [*MacDougall et al*., 2012]. Driven by large uncertainties in size, distribution, and vulnerability, models have been slow to embrace the Yedoma region OC pool. *Koven et al*. [2011] suggest that the Yedoma region, located in Siberia's coldest parts, may not thaw substantially in the near future. However, field data and maps (Figure 1) suggest that both Yedoma and thermokarst deposits occur across a wide mean annual ground temperature range, from −15°C (Figure 1, site 10) to −3°C (Figure 1, site 19). Current global-scale models are limited because they only implement one-dimensional vertical thaw; rapid subgrid-cell processes such as thermokarst and erosion with strong lateral dynamics are disregarded. However, these processes are essential for understanding and projecting the response of ice- and organic-rich permafrost to warming. Implementation of a wide range of permafrost thaw processes is needed for realistic permafrost and global carbon cycle modeling.

5. Conclusion

[21] In conclusion, based on a bootstrapping-mean approach of a large number of field samples, we confirm a substantial frozen OC pool of ~211 +160/−153 Gt in the Yedoma region, stored in Yedoma and frozen thermokarst deposits. We also suggest that this pool size may have been previously overestimated [*Zimov et al*., 2006]. Furthermore, we propose a ~2:3 ratio between the Yedoma deposit and thermokarst deposit OC pools. Thawing portions of these significant OC pools will amplify climate change in a warmer Arctic. To further improve OC calculation, sensitivity

analysis revealed that especially more data on deposit thickness will reduce Yedoma region OC pool uncertainty.

[22] **Acknowledgments.** We acknowledge support of this research by the German Ministry of Science and Education (project "System Laptev Sea" and grant 01DM12011). T. Opel, M. Z. Kanevskiy, Y. L. Shur, E.A.G. Schuur, and K. M. Walter Anthony are acknowledged for comments on the manuscript. We also thank the many Russian, U.S., and German partners who were involved in field research in the Siberian and Alaskan Arctic, and F. Günther for providing high-resolution satellite images. J.S. thanks the German National Academic Foundation for financial support. G.G. was supported by NSF OPP 0732735 and NASA NNX08AJ37G.

[23] The Editor thanks two anonymous reviewers for their assistance in evaluating this paper.

References

Battle, M., M. L. Bender, P. P. Tans, J. W. C. White, J. T. Ellis, T. Conway, and R. J. Francey (2000), Global carbon sinks and their variability inferred from atmospheric O_2 and $\delta^{13}C$, *Science*, *287*(5462), 2467–2470, doi:10.1126/science.287.5462.2467.

Burke, E. J., I. P. Hartley, and C. D. Jones (2012), Uncertainties in the global temperature change caused by carbon release from permafrost thawing, *The Cryosphere*, *6*(5), 1063–1076, doi:10.5194/tc-6-1063-2012.

Ciais, P., et al. (2012), Large inert carbon pool in the terrestrial biosphere during the Last Glacial Maximum, *Nat. Geosci.*, *5*(1), 74–79, doi:10.1038/ngeo1324.

Cory, R. M., B. C. Crump, J. A. Dobkowski, and G. W. Kling (2013), Surface exposure to sunlight stimulates CO_2 release from permafrost soil carbon in the Arctic, *Proc. Natl. Acad. Sci. U. S. A.*, *110*(9), 3429–3434, doi:10.1073/pnas.1214104110.

DeConto, R. M., S. Galeotti, M. Pagani, D. Tracy, K. Schaefer, T. Zhang, D. Pollard, and D. J. Beerling (2012), Past extreme warming events linked to massive carbon release from thawing permafrost, *Nature*, *484*(7392), 87–91, doi:10.1038/nature10929.

Dutta, K., E. A. G. Schuur, J. C. Neff, and S. A. Zimov (2006), Potential carbon release from permafrost soils of Northeastern Siberia, *Global Change Biol.*, *12*(12), 2336–2351, doi:10.1111/j.1365-2486.2006.01259.x.

Grosse, G., et al. (2011), Vulnerability of high-latitude soil organic carbon in North America to disturbance, *J. Geophys. Res.*, *116*, G00K06, doi:10.1029/2010JG001507.

Grosse, G., J. E. Robinson, R. Bryant, M. D. Taylor, W. Harper, A. DeMasi, E. Kyker-Snowman, A. Veremeeva, L. Schirrmeister, and J. Harden (2013), Distribution of late Pleistocene ice-rich syngenetic permafrost of the Yedoma Suite in east and central Siberia, Russia, *U.S.G.S. Open File Report*, *1078*, 37.

Jorgenson, M. T., K. Yoshikawa, M. Kanveskiy, Y. Shur, V. Romanovsky, S. Marchenko, G. Grosse, J. Brown, and B. Jones (2008), Permafrost characteristics of Alaska, *Proceedings of the Ninth International Conference on Permafrost*, *3*, 121–122.

Kanevskiy, M., Y. Shur, D. Fortier, M. T. Jorgenson, and E. Stephani (2011), Cryostratigraphy of late Pleistocene syngenetic permafrost (Yedoma) in northern Alaska, Itkillik River exposure, *Quat. Res.*, *75*(3), 584–596, doi:10.1016/j.yqres.2010.12.003.

Knoblauch, C., C. Beer, A. Sosnin, D. Wagner, and E.-M. Pfeiffer (2013), Predicting long-term carbon mineralization and trace gas production from thawing permafrost of Northeast Siberia, *Global Change Biol.*, *19*(4), 1160–1172, doi:10.1111/gcb.12116.

Koven, C. D., B. Ringeval, P. Friedlingstein, P. Ciais, P. Cadule, D. Khvorostyanov, G. Krinner, and C. Tarnocai (2011), Permafrost carbon-climate feedbacks accelerate global warming, *Proc. Natl. Acad. Sci. U. S. A.*, *108*(36), 14,769–14,774, doi:10.1073/pnas.1103910108.

Lantuit, H., et al. (2012), The Arctic coastal dynamics database: A new classification scheme and statistics on Arctic permafrost coastlines, *Estuar. Coast*, *35*(2), 383–400, doi:10.1007/s12237-010-9362-6.

Lee, H., E. A. G. Schuur, K. S. Inglett, M. Lavoie, and J. P. Chanton (2012), The rate of permafrost carbon release under aerobic and anaerobic conditions and its potential effects on climate, *Global Change Biol.*, *18*(2), 515–527, doi:10.1111/j.1365-2486.2011.02519.x.

MacDougall, A. H., C. A. Avis, and A. J. Weaver (2012), Significant contribution to climate warming from the permafrost carbon feedback, *Nat. Geosci.*, *5*(10), 719–721, doi:10.1038/ngeo1573.

Mackelprang, R., M. P. Waldrop, K. M. DeAngelis, M. M. David, K. L. Chavarria, S. J. Blazewicz, E. M. Rubin, and J. K. Jansson (2011), Metagenomic analysis of a permafrost microbial community reveals a rapid response to thaw, *Nature*, *480*(7377), 368–371, doi:10.1038/nature10576.

McGuire, A. D., L. G. Anderson, T. R. Christensen, S. Dallimore, L. Guo, D. J. Hayes, M. Heimann, T. D. Lorenson, R. W. Macdonald, and N. Roulet (2009), Sensitivity of the carbon cycle in the Arctic to climate change, *Ecol. Monogr.*, *79*(4), 523–555, doi:10.1890/08-2025.1.

Romanovskii, N. N. (1993), *Fundamentals of Cryogenesis of Lithosphere*, pp. 336, Moscow University Press, Moscow.

Romanovsky, V. E., et al. (2010), Thermal state of permafrost in Russia, *Perm. Periglac. Process.*, *21*(2), 136–155, doi:10.1002/ppp.683.

Schaefer, K., T. Zhang, L. Bruhwiler, and A. P. Barrett (2011), Amount and timing of permafrost carbon release in response to climate warming, *Tellus B*, *63*(2), 165–180, doi:10.1111/j.1600-0889.2011.00527.x.

Schirrmeister, L., G. Grosse, S. Wetterich, P. P. Overduin, J. Strauss, E. A. G. Schuur, and H.-W. Hubberten (2011), Fossil organic matter characteristics in permafrost deposits of the northeast Siberian Arctic, *J. Geophys. Res.*, *116*, G00M02, doi:10.1029/2011JG001647.

Schneider von Deimling, T., M. Meinshausen, A. Levermann, V. Huber, K. Frieler, D. M. Lawrence, and V. Brovkin (2012), Estimating the near-surface permafrost-carbon feedback on global warming, *Biogeosciences*, *9*(2), 649–665, doi:10.5194/bg-9-649-2012.

Schuur, E. A. G., J. G. Vogel, K. G. Crummer, H. Lee, J. O. Sickman, and T. E. Osterkamp (2009), The effect of permafrost thaw on old carbon release and net carbon exchange from tundra, *Nature*, *459*(7246), 556–559, doi:10.1038/nature08031.

Schuur, E. A. G., et al. (2013), Expert assessment of vulnerability of permafrost carbon to climate change, *Clim. Change*, *119*, 359–374, doi:10.1007/s10584-013-0730-7.

Strauss, J., L. Schirrmeister, S. Wetterich, A. Borchers, and S. P. Davydov (2012), Grain-size properties and organic-carbon stock of Yedoma Ice Complex permafrost from the Kolyma lowland, northeastern Siberia, *Glob. Biogeochem. Cycles*, *26*, GB3003, doi:10.1029/2011GB004104.

Tarnocai, C., J. G. Canadell, E. A. G. Schuur, P. Kuhry, G. Mazhitova, and S. Zimov (2009), Soil organic carbon pools in the northern circumpolar permafrost region, *Glob. Biogeochem. Cycles*, *23*, GB2023, doi:10.1029/2008GB003327.

Walter, K. M., S. A. Zimov, J. P. Chanton, D. Verbyla, and F. S. Chapin (2006), Methane bubbling from Siberian thaw lakes as a positive feedback to climate warming, *Nature*, *443*(7), 71–75, doi:10.1038/nature05040.

Zimov, S. A., S. P. Davydov, G. M. Zimova, A. I. Davydova, E. A. G. Schuur, K. Dutta, and F. S. Chapin (2006), Permafrost carbon: Stock and decomposability of a globally significant carbon pool, *Geophys. Res. Lett.*, *33*, L20502, doi:10.1029/2006GL027484.